Bond disproportionation and dynamical charge fluctuations in the perovskite rare-earth nickelates

R. J. Green,[1,2,3,*] M. W. Haverkort,[3] and G. A. Sawatzky[1,2]

[1]*Department of Physics and Astronomy, University of British Columbia, Vancouver, Canada V6T 1Z1*

[2]*Quantum Matter Institute, University of British Columbia, Vancouver, Canada V6T 1Z4*

[3]*Max Planck Institute for Chemical Physics of Solids, Nöthnitzerstraße 40, 01187 Dresden, Germany*

(Received 26 May 2016; published 15 November 2016)

We present a theory describing the local electronic properties of the perovskite rare-earth nickelates—materials which have negative charge transfer energies, strong O $2p$ – Ni $3d$ covalence, and breathing-mode lattice distortions at the origin of highly studied metal-insulator and antiferromagnetic ordering transitions. Utilizing a full-orbital, full-correlation double-cluster approach, we find strong charge fluctuations, in agreement with a bond disproportionation interpretation. The double-cluster formulation permits the inclusion of necessary orbital degeneracies and Coulomb interactions to calculate resonant x-ray spectral responses, with which we find excellent agreement with well-established experimental results. This previously absent, crucial link between theory and experiment provides validation of the recently proposed bond disproportionation theory, and provides an analysis methodology for spectroscopic studies of engineered phases of nickelates and other high-valence transition-metal compounds.

DOI: 10.1103/PhysRevB.94.195127

The perovskite rare-earth nickelate compounds ($\mathcal{R}NiO_3$) possess a rich phase diagram, exhibiting metal-insulator and antiferromagnetic ordering transitions with temperatures tunable via the rare-earth ionic size [1]. The transition into the low-temperature insulating phase is concomitant with a structural change where alternating NiO_6 octahedra are expanded and compressed in a rocksalt-pattern breathing-mode distortion [see Fig. 1(a)]. Below the Néel temperature in this distorted phase, the nickelates are E'-type antiferromagnets, with an uncommon $\mathbf{q} = (1/4, 1/4, 1/4)$ ordering vector. Remarkably, pressure [1], strain [2–5], reduced dimensionality [6,7], and the engineering of various heterointerfaces [8–11] have all been found to tune the ground state in various ways. Such a diversity of control mechanisms driving fascinating and useful emergent properties has fueled a wealth of interest in the nickelates in recent years.

A key feature of the nickelates is the unusually high formal 3+ oxidation state imposed on the Ni ions. Oxides with Ni^{3+} ($3d^7$) ions are relatively rare, and recent work suggests that the Ni here has a valence closer to 2+, with compensatory holes present in the oxygen $2p$ band. Having such a negative charge transfer energy [12] in the Zaanen-Sawatzky-Allen (ZSA) classification scheme [13,14], the nickelates can accordingly be described as *self-doped* Mott insulators [15]. Theoretical studies which assume a negative charge transfer energy *a priori*, find a novel explanation for the metal-insulator transition in the form of bond disproportionation [16–21]. Here, in the low-temperature insulating phase, the self-doped oxygen $2p$ holes mix strongly with alternating Ni sites, leading to a rocksalt-type superlattice distortion which can be identified roughly as collapsed $d^8\underline{L}^2$ and expanded $d^8\underline{L}^0$ Ni-O octahedra (where $\underline{L}$ denotes a ligand hole). A strong antiferromagnetic interaction between the ligand and Ni holes then leads to reduced moments on the collapsed octahedra, such that short and long bond Ni have spins tending toward $S = 0$ and 1, respectively.

With indications of such an uncommon electronic structure at the origin of fascinating macroscopic phenomena, experiments which can directly probe the relevant properties of the nickelates are crucial. X-ray absorption spectroscopy (XAS) at the Ni $L_{2,3}$ edge is one such technique, having strong sensitivity to the metal-insulator transition (MIT) and negative charge transfer behavior [22,23], and clear trends exist in the XAS when moving across the phase diagram [23,24]. Closely related to the XAS is the resonant magnetic diffraction (RMD) response, which probes the antiferromagnetic ordering by studying the magnetic Bragg reflection with photon energies tuned to the Ni $L_{2,3}$ resonance. Recent studies have used XAS and RMD to characterize variations of the MIT due to strain [3,25], to examine orbital polarization effects [8,26], and to study the collinearity of the magnetic moments [4,27]. However, while XAS and RMD show strong sensitivity to the electronic and magnetic structures, a satisfactory theoretical interpretation of each has yet to emerge. On one hand, the bond disproportionation models studied to date do not include the necessary orbital degeneracies for core level spectroscopy analysis (and accordingly have yet to be verified experimentally). On the other hand, the typical single-cluster model approaches which are used for spectroscopy falter due to the negative charge transfer energy and breathing distortion. A bond disproportionation model which could be tested against XAS and RMD would simultaneously provide validation of the theory and a way to thoroughly analyze the ubiquitous, detailed spectra which have emerged from both bulk nickelates and engineered heterostructures [2–4,8–10,22–27].

In this work, we formulate a full-correlation, double-cluster model to describe the insulating and magnetic phases of the nickelates. The formulation permits the inclusion of negative charge transfer, bond and charge disproportionation, and, most importantly, the necessary orbital degeneracies and Coulomb interactions to simulate core level spectroscopy, providing a key test of bond disproportionation against resonant x-ray experiments. Our approach finds the same instability toward $d^8\underline{L}^2$ ($S = 0$) and $d^8\underline{L}^0$ ($S = 1$) alternating octahedra in the presence of a breathing distortion that was found in recent

*rgreen@phas.ubc.ca

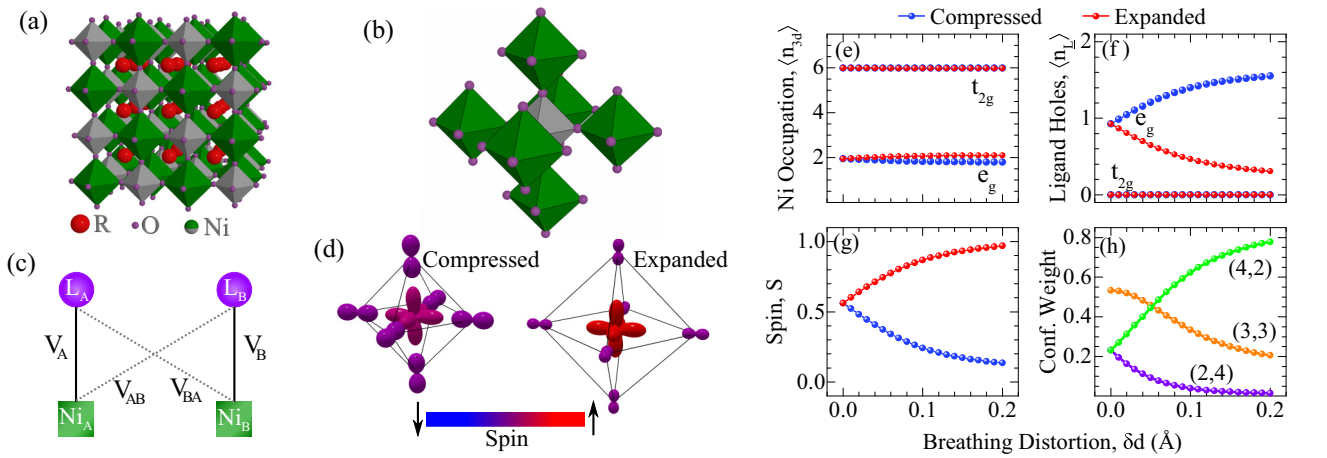

FIG. 1. (a) Perovskite nickelate structure with alternating octahedra shaded to distinguish the long (green) and short (gray) bond sites in the low-temperature distorted phase. (b) A cutout of the structure demonstrating the O_h arrangement of the two octahedra types. (c) Diagrammatic depictions of the hopping arrangements for the double-cluster model. (d) Visualization of calculated hole density matrices on compressed (left) and expanded (right) octahedra in the distorted phase (ligand hole densities are scaled by a factor of 2 for clarity). (e)–(h) Ground-state characteristics from the double-cluster model: (e) Distribution of Ni $3d$ electrons. (f) Distribution of ligand holes. (g) Spins for the two octahedra. (h) Weights of configurations with hole distributions (n_A,n_B) on the compressed and expanded octahedra, respectively.

restricted-orbital studies. Further, we find moment sizes for each sublattice in agreement with those determined experimentally. At the same time, we find spectral responses for XAS and RMD which are in excellent agreement with experiment, including pronounced trends across the rare-earth series. While the model provides a previously missing validation of bond disproportionation against experiment, it is also a powerful tool for the precise analysis of engineered phases of nickelates as well as many other high-valence transition-metal oxides.

In Fig. 1(a), we depict the prototypical structure of the nickelates. Alternating octahedra are shaded to distinguish the long and short bond NiO_6 octahedra present in the breathing-mode distorted insulating phase. This distortion forms a rocksalt pattern, with each long (short) bond octahedron surrounded by six short (long) bond octahedra in an O_h symmetric manner as exemplified in Fig. 1(b). To enable a calculation which includes the full Coulomb interactions necessary for spectroscopy simulations, we develop a model similar to the multiplet ligand field theory approximation, which has had great success in this area [28,29]. However, instead of the typical approach of exact diagonalization on a single NiO_6 cluster, we create two clusters, one representing each sublattice of the rocksalt distortion. Each of our two Ni-O octahedral clusters are constructed from a standard ligand field theory Hamiltonian, including all local $3d$ (and Ni $2p$) Coulomb interactions, crystal fields, $3d$-ligand hybridization, and spin-orbit interaction [30]. Recalling the rocksalt pattern formed by the two distinct octahedra in the solid, we then couple our two cluster models via O_h symmetric hybridization operators (having e_g and t_{2g} symmetry). The coupling is shown diagrammatically in Fig. 1(c). The individual clusters have standard ligand field Ni-ligand hopping V_A and V_B, and intercluster Ni-ligand hopping is shown as V_{AB} and V_{BA}. The general form of our Hamiltonian is then $H = H_{LF_A} + H_{LF_B} + H_{\mathrm{mix}}$, where the first two terms are the independent ligand field Hamiltonians for the two distinct octahedra, and the final term introduces the O_h-symmetric mixing (full details of the Hamiltonian and parameters are presented in the Supplemental Material [30]). The breathing distortion is introduced into the model by a modulation of the hopping and crystal-field terms, according to Harrison's rules [19,20,30,31]. The computations are performed with our exact-diagonalization code, QUANTY [28,32–34].

Figures 1(d)–1(h) display the ground-state properties of the model as a function of the breathing distortion, δd. We parametrize the distortion as the difference in long and short bond lengths d_L and d_S from the mean value d_0 ($d_{L/S} = d_0 + / - \delta d$). In Fig. 1(e), we find that very little change in the Ni $3d$ occupation occurs via the breathing distortion. The t_{2g} orbitals stay fully occupied and only a minor variation of the e_g occupation occurs, with a total average occupation of ~8 electrons per Ni, consistent with the negative charge transfer scenario [35].

The oxygen orbitals, in contrast to the Ni, are very active under the breathing distortion. As shown in Fig. 1(f), with no distortion, there is one (self-doped) e_g ligand hole per cluster. However, the holes shift to the compressed octahedron when the breathing distortion is introduced. This action of the oxygen holes leads to a reduction of the spin on the compressed octahedron, as shown in Fig. 1(g), since the holes are strongly antiferromagnetically coupled to the holes in the Ni $3d$ shell. This leaves the expanded octahedron Ni unscreened, and its spin accordingly approaches $S = 1$, the expected value for a high spin, ionic $3d^8$ configuration. For $HoNiO_3$, where breathing distortions and spin moments have been measured experimentally [36,37], we find good agreement. The general behavior of Figs. 1(e)–1(g), summarized pictorially for $\delta d =$ 0.05 Å in Fig. 1(d), also agrees with recent theory studies which were restricted to the active e_g orbital basis [18–20].

Overall, the calculations show a clear transition from a (3,3) hole occupation of the two octahedra toward a (4,2) hole arrangement for the compressed and expanded octahedra, respectively, with spins accordingly transitioning from $(^1/_2,^1/_2)$ to (0,1). This transition is detailed in Fig. 1(h), where we

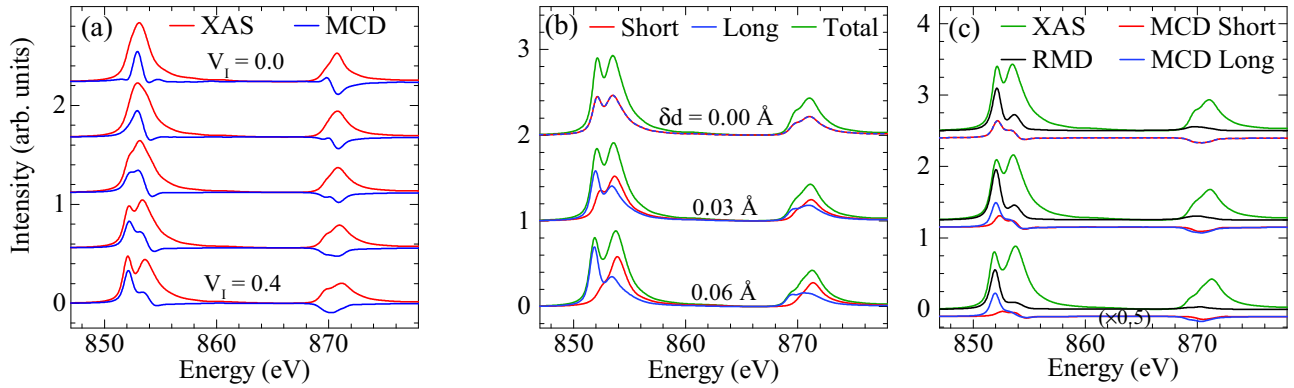

FIG. 2. Resonant x-ray responses of the double-cluster model. (a) XAS and MCD spectra are shown in the single-cluster limit (top, intercluster hopping V_I set to zero), and for increasing intercluster hopping values. (b) XAS spectra for different magnitudes of the breathing distortion (with $V_I = 0.35$). The spectra of the two inequivalent sites are shown, along with their sum. (c) Resonant magnetic diffraction and site-decomposed MCD spectra are shown for the same breathing distortions as (b), along with the total XAS for comparison. MCD spectra are offset for clarity.

plot the projection of the ground state onto the relevant basis states. We emphasize that even with no breathing distortion, a dynamic charge ordering is present, while the bond disproportionated configuration (4,2) dominates the ground state for large distortions.

In Fig. 2, we show the resonant soft x-ray responses of our model, which has the full Ni $3d$ and $2p$ orbital degeneracies and their Coulomb interactions necessarily included in order to capture the detailed multiplet features in the spectra. In Fig. 2(a), we compare the double-cluster model (with no breathing distortion) to a conventional single-cluster model, where the intercluster hopping V_I is set to zero. Increasing V_I from zero leads to a pronounced first peak being separated out below both the L_3 and L_2 edges. Such a peak is a distinct characteristic of the insulating nickelates [24] and, importantly, we find that the peak also has a strong magnetic circular dichroism (MCD) signal, consistent with RMD experiments which find the magnetic diffraction to be strongest at that peak [4,27,38]. Given that no breathing distortion is introduced yet in this plot, the peak arises due to nonlocal excitations between the two clusters. Such an effect is perhaps not surprising, given the negative charge transfer energy and strong covalence, but it demonstrates that even in the absence of breathing distortions, a proper interpretation of the spectra of high-valence transition-metal oxides might require at least a double-cluster model where such excitations can be captured. Similar intersite effects requiring extensions beyond the single-cluster approximation were recently identified in the XAS of strongly covalent mixed-valence systems [39]. We note that our value of $V_I = 0.35$ is slightly less than one might expect for 180 degree bonds between adjacent Ni atoms [30], in accordance with octahedral tilting that is present in the real materials.

Figure 2(b) shows the effect of the breathing distortion on the XAS spectra. In the presence of the distortion, there are distinct spectra for the two inequivalent sites, and as such we show these two spectra, along with their sum. Here it is evident that the spectrum from the long (short) bond octahedron shifts to lower (higher) energies as the breathing distortion is increased. In the extreme case, the sharp prepeak arises entirely from the long bond Ni. This trend is in excellent agreement with the nickelate phase diagram, where smaller rare earths lead to larger breathing distortions and a larger separation of the XAS peaks [23,24].

Figure 2(c) details the magnetic response for the same three breathing distortions of Fig. 2(b). The total XAS is shown again for comparison, and the site-decomposed MCD spectra are shown. Consistent with the tendency toward $S = 0$ and $S = 1$ moments on the short and long bond sites, as was shown in Fig. 1, the MCD spectrum of the long (short) bond site becomes stronger (weaker) as the breathing distortion is introduced. As the long bond site contributes the most to the sharp first peak, the MCD response is then concentrated mostly on that peak as well. For comparison to experiment, we also show the calculated resonant magnetic diffraction (RMD) response, which peaks strongly at the XAS first peak and has a weak shoulder at higher energies, in excellent agreement with previous experiments [4,27,38].

The effects of intercluster hopping on the XAS spectra of Fig. 2(a) demonstrate the importance of nonlocal excitations and suggest a highly covalent nature of the ground state captured in our double-cluster model. We verify this in Fig. 3 by a decompositional analysis of the ground-state wave function. In conventional single-cluster configuration interaction theory, the ground state is thus given by $|\psi_0\rangle = \sum_i c_i |d^{n+i}\underline{L}^i\rangle$, where c_i^2 gives the weight of configuration i. In the nickelates, $n = 7$, and one is therefore limited to four configurations. The weight of these configurations in the single-cluster limit of our model is plotted on the right in Fig. 3(a). In green we show the calculations including electron-electron correlations, i.e., the Hamiltonian including the full Coulomb interaction is solved by exact diagonalization. In red we show the weight of the different configurations approximating the Coulomb interaction by a potential as one would do in a local density or Hartree-Fock approximation. Correlations induced by the Coulomb interaction reduce the amount of charge fluctuations. One configuration gains more weight, reducing the weight of all others and thus changing the variance of the Ni d electron count. Interestingly it is not the $|d^7\underline{L}^0\rangle$ configuration that gains the most weight in the strongly correlated limit, but the $|d^8\underline{L}^1\rangle$

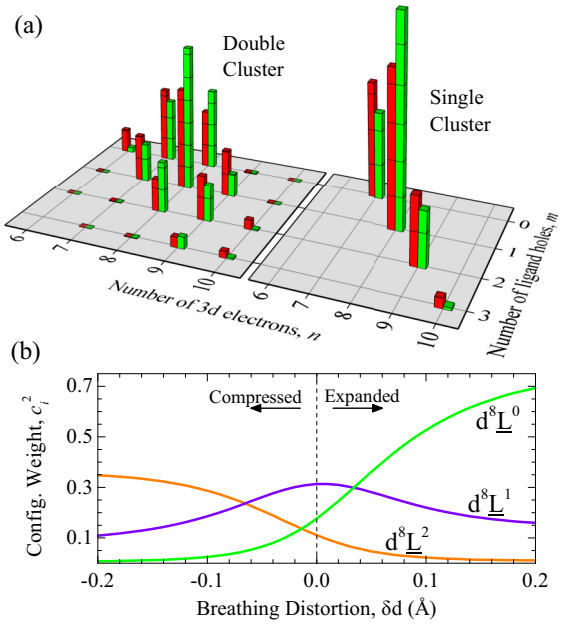

FIG. 3. (a) Configuration weights c_i^2 are compared for the present double-cluster model (left, green) and conventional ligand field theory (right, green), demonstrating the additional determinants which arise in negative charge transfer situations not captured by single-cluster theory. In both cases, the weights for the noninteracting approximation are shown in red for comparison. Divisions on the bars have values of 0.05 for the double cluster and 0.10 for the single cluster. (b) The compressed octahedron exhibits a wave function with dominant ligand hole-rich d^8 determinants, while the expanded octahedron has a much more ionic wave function.

configuration. The local symmetry is still that of a $|d^7\underline{L}^0\rangle$ configuration, i.e., $\langle S^2\rangle = 3/4$, and one has a local doublet, defining the formal valence to be Ni^{3+}.

In the double-cluster model, many more configurations are possible ($d^n\underline{L}^m$, in general) due to charge fluctuations between the clusters. We plot the configuration weights for the double-cluster model with no breathing distortion on the left in Fig. 3(a). Again correlations (green) reduce the amount of charge fluctuations on the Ni site and, like the single-cluster calculation, the d^8 configurations have the most weight. The ligand charge fluctuations are not reduced between the correlated (green) and uncorrelated (red) calculations. The local state can thus be thought of as a superposition of $|d^8\underline{L}^0\rangle$, $|d^8\underline{L}^1\rangle$, and $|d^8\underline{L}^2\rangle$. Magnetically, the local cluster state is thus a superposition of a triplet, doublet and singlet with Ni-ligand cluster formal valences of 2+, 3+, and 4+, respectively.

In Fig. 3(b), we show the effects of the breathing distortion on the d^8 derived configurations of the double-cluster model. As demonstrated above, for no breathing distortion there is a strong mixture of configurations (high covalency). However, upon the introduction of the breathing distortion, the ligand hole character strongly shifts, such that the compressed octahedron has mostly $d^8\underline{L}^2$ (and, to a lesser extent, $d^8\underline{L}^1$) character [reflecting what was shown in Fig. 1(f)]. The expanded octahedron, however, becomes much more ionic, being dominated by the $d^8\underline{L}^0$ configuration. It is this ionic character of the long bond sublattice which has led to suggestions that the nickelate MIT can be described as a *site-selective* Mott transition [18]. Alternatively, given the active oxygen electronic structure due to the negative charge transfer energy, and the lattice breathing distortion, the MIT might be more aptly described as Peierls-like.

Our double-cluster model bridges the gap between electronic structure experiments and theories of negative charge transfer and bond disproportionation in the rare-earth nickelates. By accounting for self-doped holes in the oxygen $2p$ band as well as structural breathing distortions, we find pronounced bond disproportionation effects in the ground state, including unequal spin moments on the two sublattices, in excellent agreement with experiments. Additionally, we show the effect of bond disproportionation on the soft x-ray spectral response, again finding excellent agreement with experiment and providing a tool for future studies of engineered phases. The highly covalent wave functions and nonlocal excitations captured by the double-cluster model developed here show that it will be important for other high oxidation state transition-metal oxides, even in the absence of breathing distortions. New insights into highly studied materials such as perovskite manganates, ferrates, cobaltates, etc. and their resonant scattering responses should also be captured by the model.

Note added in proof. Recently, an experimental study was published [40] which supports the negative charge transfer character of the nickelates as used in our theoretical model here.

We thank M. Hepting, E. Benckiser, Y. Lu, I. Elfimov, M. Berciu, T. Schmitt, and V. Bisogni for helpful discussions. This work was supported by Natural Sciences and Engineering Research Council of Canada, CIfAR, and the Max Planck - UBC Centre for Quantum Materials.

[1] M. L. Medarde, J. Phys.: Condens. Matter **9**, 1679 (1997).
[2] S. Catalano, M. Gibert, V. Bisogni, O. E. Peil, F. He, R. Sutarto, M. Viret, P. Zubko, R. Scherwitzl, A. Georges, G. A. Sawatzky, T. Schmitt, and J.-M. Triscone, APL Mater. **2**, 116110 (2014).
[3] J. Liu, M. Kareev, B. Gray, J. W. Kim, P. Ryan, B. Dabrowski, J. W. Freeland, and J. Chakhalian, Appl. Phys. Lett. **96**, 233110 (2010).
[4] A. Frano, E. Schierle, M. W. Haverkort, Y. Lu, M. Wu, S. Blanco-Canosa, U. Nwankwo, A. V. Boris, P. Wochner, G. Cristiani, H. U. Habermeier, G. Logvenov, V. Hinkov, E. Benckiser, E. Weschke, and B. Keimer, Phys. Rev. Lett. **111**, 106804 (2013).
[5] J. Liu, M. Kargarian, M. Kareev, B. Gray, P. J. Ryan, A. Cruz, N. Tahir, Y.-D. Chuang, J. Guo, J. M. Rondinelli, J. W. Freeland, G. A. Fiete, and J. Chakhalian, Nat. Commun. **4**, 2714 (2013).
[6] A. V. Boris, Y. Matiks, E. Benckiser, A. Frano, P. Popovich, V. Hinkov, P. Wochner, M. Castro-Colin, E. Detemple, V. K. Malik, C. Bernhard, T. Prokscha, A. Suter, Z. Salman, E. Morenzoni,

G. Cristiani, H.-U. Habermeier, and B. Keimer, Science **332**, 937 (2011).
[7] M. Hepting, M. Minola, A. Frano, G. Cristiani, G. Logvenov, E. Schierle, M. Wu, M. Bluschke, E. Weschke, H.-U. Habermeier, E. Benckiser, M. Le Tacon, and B. Keimer, Phys. Rev. Lett. **113**, 227206 (2014).
[8] E. Benckiser, M. W. Haverkort, S. Brueck, E. Goering, S. Macke, A. Frano, X. Yang, O. K. Andersen, G. Cristiani, H.-U. Habermeier, A. V. Boris, I. Zegkinoglou, P. Wochner, H.-J. Kim, V. Hinkov, and B. Keimer, Nat. Mater. **10**, 189 (2011).
[9] A. S. Disa, D. P. Kumah, A. Malashevich, H. Chen, D. A. Arena, E. D. Specht, S. Ismail-Beigi, F. J. Walker, and C. H. Ahn, Phys. Rev. Lett. **114**, 026801 (2015).
[10] S. Middey, J. Chakhalian, P. Mahadevan, J. Freeland, A. Millis, and D. Sarma, Annu. Rev. Mater. Res. **46**, 305 (2016).
[11] H. Chen, D. P. Kumah, A. S. Disa, F. J. Walker, C. H. Ahn, and S. Ismail-Beigi, Phys. Rev. Lett. **110**, 186402 (2013).
[12] T. Mizokawa, H. Namatame, A. Fujimori, K. Akeyama, H. Kondoh, H. Kuroda, and N. Kosugi, Phys. Rev. Lett. **67**, 1638 (1991).
[13] J. Zaanen, G. A. Sawatzky, and J. W. Allen, Phys. Rev. Lett. **55**, 418 (1985).
[14] Most studies (including Refs. [12,13], for example) define the charge transfer energy as the energy difference between the center of the oxygen $2p$ band and the center of the upper Hubbard $3d$ band. For small and negative charge transfer energies such as in the present work, the quantity of interest is the energy separation between the *top* of the oxygen band and the *bottom* of the $3d$ band. Often called the effective charge transfer energy, this quantity can also be defined as the smallest energy difference between d^n and $d^{n+1}\underline{L}$ configurations.
[15] M. A. Korotin, V. I. Anisimov, D. I. Khomskii, and G. A. Sawatzky, Phys. Rev. Lett. **80**, 4305 (1998).
[16] T. Mizokawa, D. I. Khomskii, and G. A. Sawatzky, Phys. Rev. B **61**, 11263 (2000).
[17] I. I. Mazin, D. I. Khomskii, R. Lengsdorf, J. A. Alonso, W. G. Marshall, R. M. Ibberson, A. Podlesnyak, M. J. Martínez-Lope, and M. M. Abd-Elmeguid, Phys. Rev. Lett. **98**, 176406 (2007).
[18] H. Park, A. J. Millis, and C. A. Marianetti, Phys. Rev. Lett. **109**, 156402 (2012).
[19] S. Johnston, A. Mukherjee, I. Elfimov, M. Berciu, and G. A. Sawatzky, Phys. Rev. Lett. **112**, 106404 (2014).
[20] B. Lau and A. J. Millis, Phys. Rev. Lett. **110**, 126404 (2013).
[21] A. Subedi, O. E. Peil, and A. Georges, Phys. Rev. B **91**, 075128 (2015).
[22] C. Piamonteze, H. C. N. Tolentino, F. C. Vicentin, A. Y. Ramos, N. E. Massa, J. A. Alonso, M. J. Martínez-Lope, and M. T. Casais, Surf. Rev. Lett. **09**, 1121 (2002).
[23] C. Piamonteze, F. M. F. de Groot, H. C. N. Tolentino, A. Y. Ramos, N. E. Massa, J. A. Alonso, and M. J. Martínez-Lope, Phys. Rev. B **71**, 020406 (2005).
[24] J. W. Freeland, M. van Veenendaal, and J. Chakhalian, J. Electron Spectrosc. Relat. Phenom. **208**, 56 (2015).
[25] D. Meyers, S. Middey, M. Kareev, M. van Veenendaal, E. J. Moon, B. A. Gray, J. Liu, J. W. Freeland, and J. Chakhalian, Phys. Rev. B **88**, 075116 (2013).
[26] M. Wu, E. Benckiser, M. W. Haverkort, A. Frano, Y. Lu, U. Nwankwo, S. Brück, P. Audehm, E. Goering, S. Macke, V. Hinkov, P. Wochner, G. Christiani, S. Heinze, G. Logvenov, H.-U. Habermeier, and B. Keimer, Phys. Rev. B **88**, 125124 (2013).
[27] V. Scagnoli, U. Staub, A. M. Mulders, M. Janousch, G. I. Meijer, G. Hammerl, J. M. Tonnerre, and N. Stojic, Phys. Rev. B **73**, 100409 (2006).
[28] M. W. Haverkort, M. Zwierzycki, and O. K. Andersen, Phys. Rev. B **85**, 165113 (2012).
[29] F. De Groot and A. Kotani, *Core Level Spectroscopy of Solids* (Taylor & Francis CRC Press, Boca Raton, 2008).
[30] See Supplemental Material at http://link.aps.org/supplemental/10.1103/PhysRevB.94.195127, which includes Refs. 41–44, for a complete description of the Hamiltonian and computational details.
[31] J. M. Wills and W. A. Harrison, Phys. Rev. B **28**, 4363 (1983).
[32] Y. Lu, M. Höppner, O. Gunnarsson, and M. W. Haverkort, Phys. Rev. B **90**, 085102 (2014).
[33] M. W. Haverkort, G. Sangiovanni, P. Hansmann, A. Toschi, Y. Lu, and S. Macke, Europhys. Lett. **108**, 57004 (2014).
[34] M. W. Haverkort *et al.*, http://www.quanty.org.
[35] We use a configuration-averaged charge transfer energy of $\Delta = -0.5$ eV, which yields an effective charge transfer energy between the lowest d^7 and $d^8\underline{L}$ configurations of about -0.6 eV [30].
[36] M. T. Fernández-Díaz, J. A. Alonso, M. J. Martínez-Lope, M. T. Casais, and J. L. García-Muñoz, Phys. Rev. B **64**, 144417 (2001).
[37] J. A. Alonso, M. J. Martínez-Lope, M. T. Casais, J. L. García-Muñoz, and M. T. Fernández-Díaz, Phys. Rev. B **61**, 1756 (2000).
[38] Y. Bodenthin, U. Staub, C. Piamonteze, M. García-Fernández, M. J. Martínez-Lope, and J. A. Alonso, J. Phys.: Condens. Matter **23**, 036002 (2011).
[39] S. S. Gupta, H. Wadati, and G. A. Sawatzky, Europhys. Lett. **93**, 47008 (2011).
[40] V. Bisogni, S. Catalano, R. J. Green, M. Gibert, R. Scherwitzl, Y. Huang, V. N. Strocov, P. Zubko, S. Balandeh, J.-M. Triscone, G. A. Sawatzky, and T. Schmitt, Nature Commun. **7**, 13017 (2016).
[41] C. Ballhausen, *Introduction to Ligand Field Theory* (McGraw-Hill Book Co., New York, 1962).
[42] J. Zaanen, C. Westra, and G. A. Sawatzky, Phys. Rev. B **33**, 8060 (1986).
[43] R. Cowan, *The Theory of Atomic Structure and Spectra* (University of California Press, Berkeley, 1981).
[44] E. Dagotto, Rev. Mod. Phys. **66**, 763 (1994).